Structure-based analysis of the molecular interactions between acyltransferase and acyl carrier protein in vicenistatin biosynthesis

Akimasa Miyanaga[a,1], Shohei Iwasawa[a], Yuji Shinohara[b], Fumitaka Kudo[a], and Tadashi Eguchi[b,1]

[a]Department of Chemistry, Tokyo Institute of Technology, O-okayama, Meguro-ku, Tokyo 152-8551, Japan; and [b]Department of Chemistry and Materials Science, Tokyo Institute of Technology, O-okayama, Meguro-ku, Tokyo 152-8551, Japan

Edited by Chaitan Khosla, Stanford University, Stanford, CA, and accepted by the Editorial Board January 11, 2016 (received for review October 09, 2015)

Acyltransferases (ATs) are key determinants of building block specificity in polyketide biosynthesis. Despite the importance of protein–protein interactions between AT and acyl carrier protein (ACP) during the acyltransfer reaction, the mechanism of ACP recognition by AT is not understood in detail. Herein, we report the crystal structure of AT VinK, which transfers a dipeptide group between two ACPs, VinL and VinP1LdACP, in vicenistatin biosynthesis. The isolated VinK structure showed a unique substrate-binding pocket for the dipeptide group linked to ACP. To gain greater insight into the mechanism of ACP recognition, we attempted to crystallize the VinK–ACP complexes. Because transient enzyme–ACP complexes are difficult to crystallize, we developed a covalent cross-linking strategy using a bifunctional maleimide reagent to trap the VinK–ACP complexes, allowing the determination of the crystal structure of the VinK–VinL complex. In the complex structure, Arg-153, Met-206, and Arg-299 of VinK interact with the negatively charged helix II region of VinL. The VinK–VinL complex structure allows, to our knowledge, the first visualization of the interaction between AT and ACP and provides detailed mechanistic insights into ACP recognition by AT.

polyketide | acyltransferase | acyl carrier protein | protein–protein interaction | cross-linking

Polyketide synthases (PKSs) are multifunctional enzymes responsible for the biosynthesis of various polyketide natural products (1). Bacterial modular PKSs comprise several catalytic modules that are each responsible for a single round of the polyketide chain elongation reaction. Each module minimally consists of a ketosynthase (KS) domain, an acyltransferase (AT) domain, and an acyl carrier protein (ACP) domain. The AT domain recognizes a specific acyl building block and catalyzes its transfer reaction onto the 4′-phosphopantetheine arm of the ACP. KS extends the polyketide chain by condensing the resulting ACP-bound building blocks with the elongated acyl–ACPs. Although standard modular PKSs contain AT domains in their modules, some modular PKSs lack AT domains in each module and instead receive their acyl building blocks by standalone *trans*-acting ATs (2).

The selection of the starter unit is generally governed by the substrate specificity of the AT domain in the loading module (1). In some modular PKS systems, a didomain-type loading module comprising a loading AT domain and an ACP domain selects an acyl starter building block such as an acetate unit to generate an acyl–ACP intermediate, which is transferred to the downstream extension module for polyketide chain elongation. Alternatively, in a KS_Q-type loading module consisting of three domains, the AT domain selects an α-carboxyacyl substrate such as a malonyl group, and the KS_Q domain subsequently catalyzes its decarboxylation to construct an acyl–ACP thioester. For polyketide chain elongation, the AT domain of the extension module generally recognizes a specific α-carboxyacyl–CoA as an extender building block (3). Malonyl– and methylmalonyl–CoA are commonly used as extender building blocks in biosynthetic pathways. Some ATs were reported to recognize ACP-bound substrates such as methoxymalonyl–, hydroxymalonyl–, and aminomalonyl–ACP (3, 4). Thus, ATs are key determinants of building block specificity in polyketide biosynthesis and attractive targets to change the substrate specificity to obtain biologically active unnatural polyketide products (5). However, the substitution of an AT domain by a homologous AT domain possessing different substrate specificity resulted in reduced or abolished production of polyketide analogs in many cases, probably because of disruption of proper protein–protein interactions or the inability of downstream modules to process polyketide analogs (5, 6).

The importance of protein–protein interaction between AT and ACP during the acyltransfer reaction was proposed in previous studies (7, 8). Wong et al. described that AT recognizes its cognate ACP from other ACPs through protein–protein interactions (7). Proper AT–ACP interactions are believed to be essential for kinetically efficient polyketide chain elongation. However, the mechanism of ACP recognition is not well understood because isolated AT structures provide no detailed information on the AT–ACP interactions (9). Structural determination of the AT–ACP complex is necessary for the complete understanding of the basis of ACP recognition for the acyltransfer reaction.

Significance

Acyltransferases (ATs) are responsible for the selection and incorporation of acyl building blocks in the biosynthesis of various polyketide natural products. Proper protein–protein interactions between AT and cognate acyl carrier protein (ACP) are critical for the functional transfer of acyl groups. However, the ACP recognition mechanism has remained elusive because the structural determination of an AT–ACP complex is hampered by the weak and transient interactions between them. Herein, we describe the first crystal structure of the AT–ACP complex. To stabilize the weak protein–protein interaction sufficiently for analysis, we prepared a covalent AT–ACP complex using a cross-linking reagent for crystallization. The determined AT–ACP complex structure provides detailed mechanistic insights into ACP recognition by AT.

Author contributions: A.M., F.K., and T.E. designed research; A.M., S.I., and Y.S. performed research; A.M., S.I., Y.S., F.K., and T.E. analyzed data; and A.M., F.K., and T.E. wrote the paper.

The authors declare no conflict of interest.

This article is a PNAS Direct Submission. C.K. is a guest editor invited by the Editorial Board.

Data deposition: The atomic coordinates and structure factors have been deposited in the Protein Data Bank, www.pdb.org (PDB ID codes 5CZC and 5CZD).

[1]To whom correspondence may be addressed. Email: eguchi@chem.titech.ac.jp or miyanaga.a.aa@m.titech.ac.jp.

This article contains supporting information online at www.pnas.org/lookup/suppl/doi:10.1073/pnas.1520042113/-/DCSupplemental.

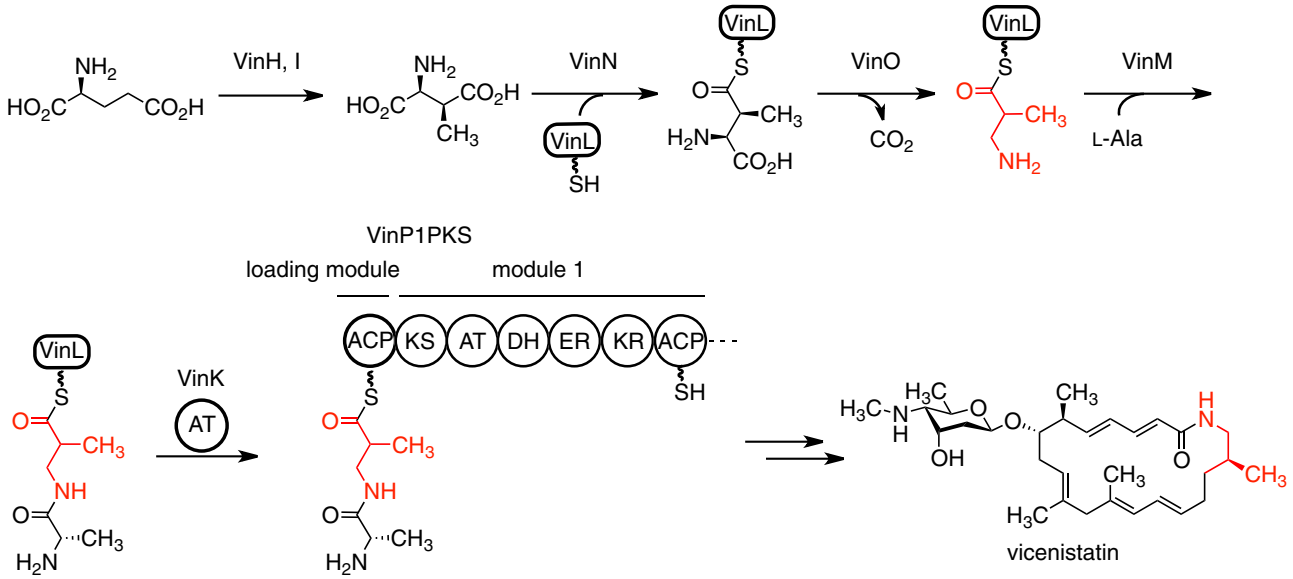

Fig. 1. Biosynthetic pathway of vicenistatin, including the VinK reaction. The 3-aminoisobutyrate unit is shown in red.

Macrolactam antibiotics are an important class of macrocyclic polyketides, and most contain a unique β-amino acid starter unit in their polyketide skeletons (10). Vicenistatin, produced by *Streptomyces halstedii* HC34, possesses a 3-aminoisobutyrate unit at the starter position of the polyketide backbone (11). This starter unit is biosynthesized from L-glutamate via (2*S*,3*S*)-3-methylaspartate, which is initially transferred onto the stand-alone ACP VinL by the adenylation enzyme VinN (12, 13). After decarboxylation, the resulting 3-aminoisobutyrate unit is aminoacylated with L-alanine to give dipeptidyl–VinL by another adenylation enzyme VinM. Then, the dipeptidyl moiety is transferred from VinL to the ACP domain (VinP1LdACP) of the VinP1PKS loading module by the *trans*-acting AT VinK (Fig. 1). These β-amino acid carrying enzymes are conserved in various macrolactam polyketide biosynthetic gene clusters, suggesting that β-amino acid starter units are loaded to PKS through the same mechanism in their biosynthesis (10).

During the dipeptide transfer reaction from VinL to VinP1LdACP, VinK is supposed to recognize the VinL region as well as the dipeptidyl moiety to overcome the kinetic disadvantage of the diffusion-controlled limit. Additionally, VinK should distinguish VinP1LdACP as an acyl acceptor from other ACPs. Thus, we assume that the specific protein–protein interaction between VinK and two ACPs is important for the reaction. However, the origins of ACP selectivity cannot be predicted from the amino acid sequence of VinK. In this study, we carried out mutational and structural studies on VinK to clarify how VinK recognizes ACPs. The covalent VinK–VinL complex structure allows, to our knowledge, the first visualization of the interactions between AT and ACP and provides detailed mechanistic insights into ACP recognition by AT.

Results

Crystal Structure of VinK. To obtain the structural basis of substrate and ACP recognition, we first determined the VinK crystal structure at 1.80-Å resolution (Table S1). VinK is organized into two domains, including a large domain (residues 19–143 and 214–319) and a small domain (residues 144–213) (Fig. 2*A*). The overall architecture of VinK is similar to those of other structurally characterized ATs including FabD [Protein Data Bank (PDB) ID code 2G2Z; 25% sequence identity; 3.0-Å root mean square deviation (rmsd) for Cα atoms], which is a discrete malonyl–CoA:ACP transacylase (MCAT) of *Escherichia coli* fatty acid synthase (FAS) (14), malonyl–CoA-specific *trans*-acting AT

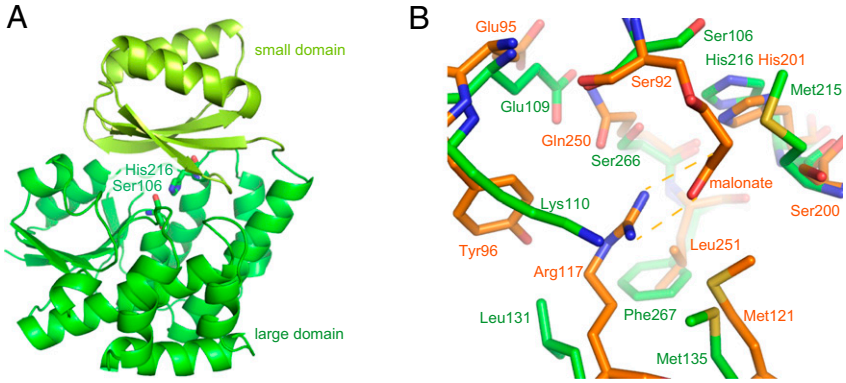

Fig. 2. Structure of VinK. (*A*) Overall structure of VinK. The large and small domains are shown in green and yellow-green, respectively. The catalytic residues are shown as sticks. (*B*) The structure of the substrate-binding pocket. The superimposed structures of VinK (green) and FabD (orange; PDB ID code 2G2Z) are shown. In the FabD structure, the malonyl moiety is covalently bound to the catalytic Ser-92.

(PDB ID code 3RGI; 21% sequence identity; 2.6 Å rmsd for Cα atoms) from disorazole synthase (DSZS) (15), and ZmaA AT (PDB ID code 4QBU; 18% sequence identity; 3.6 Å rmsd for Cα atoms), which recognizes hydroxymalonyl–ACP as a substrate (4).

VinK has two conserved catalytic residues, Ser-106 and His-216, at the interface between the large domain and small domain as observed in other ATs (Fig. 2*A* and Fig. S1). The substrate-binding cavity of VinK is constructed by residues Glu-109, Lys-110, Leu-131, Met-135, Met-215, Ser-266, and Phe-267, which are located in the large domain (Fig. 2*B* and Fig. S2). FabD has an Arg-117 at the substrate-binding cavity for the recognition of the carboxyl group of the malonate substrate (14), whereas VinK has a Leu-131 at the corresponding position (Fig. 2*B* and Fig. S1). This Leu-131 residue swings away from the catalytic Ser-106 and appears to provide the space for the bulky dipeptidyl moiety. Thus, VinK seems to have a larger substrate-binding tunnel than that of malonyl–CoA-specific ATs.

Cross-Linking Reaction to Obtain VinK–ACP Complexes. To gain greater insight into how VinK recognizes ACPs during the reaction, we attempted to crystallize VinK–VinL and –VinP1LdACP complexes. Because transient enzyme–ACP complexes are generally difficult to crystallize, we designed a site-specific covalent cross-linking method using bifunctional maleimide reagents for trapping the VinK–ACP complexes. We introduced the Cys mutation at the position of Ser-266, which is a noncatalytic residue at the base of the substrate-binding tunnel in VinK (Fig. 2*B*) and then used this S266C mutant for cross-linking to the 4′-phosphopantetheine arm of ACPs. The cross-linking reaction between the VinK S266C mutant and VinL in the presence of 1,2-bismeleimidoethane (BMOE) gave a covalent complex in sufficient yield (Fig. 3). In contrast, no apparent cross-linking was observed between the VinK wild type and VinL. This result suggested that the specific cross-link formation occurred at the substrate-binding pocket of the VinK S266C mutant. Similarly, the cross-linking reaction between the VinK S266C mutant and VinP1LdACP in the presence of BMOE gave a covalent complex (Fig. S3*A*). Next, we purified these covalent VinK–VinL and –VinP1LdACP complexes for crystallization (Fig. S3*B*). We obtained reproducible VinK–VinL complex crystals, although we failed to obtain a VinK–VinP1LdACP crystal. The mixture of the VinK S266C mutant with VinL in the absence of BMOE did not give any complex crystals, indicating the necessity of using BMOE to capture VinL.

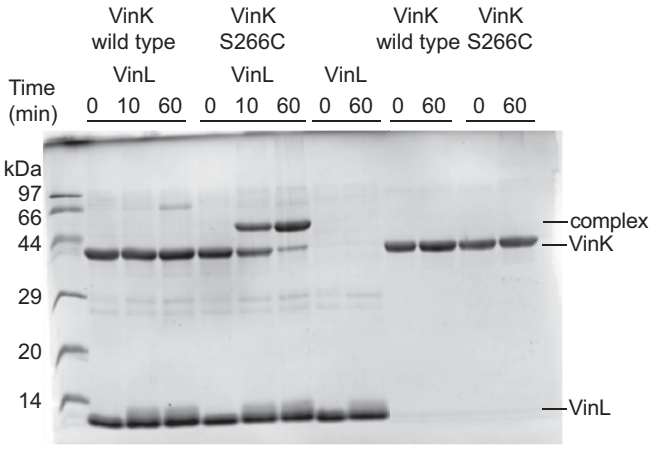

Fig. 3. Cross-linking reaction of VinK with VinL in the presence of BMOE. SDS/PAGE after the reaction of VinK with VinL for 10 and 60 min is shown. The bands corresponding to the complex formation are evident in the reaction mixture of the VinK S266C mutant with VinL.

Crystal Structure of the VinK–VinL Complex. We determined the crystal structure of the VinK–VinL complex at 2.34-Å resolution (Table S1). In the complex structure, one VinK molecule and one VinL molecule are present in the crystallographic asymmetric unit (Fig. 4*A*). The overall architecture of VinL is similar to those of other structurally characterized carrier proteins (CPs) including *E. coli* FAS ACP (AcpP) (PDB ID code 2FAE; 21% sequence identity; 2.0 Å rmsd for Cα atoms; ref. 16). VinL has a helix bundle fold with three major helices (helices I, II, and III) and one minor distorted helix III′, as observed in most of the known ACP structures (9). A 4′-phosphopantetheine arm is covalently attached to Ser-36, which is located at the beginning of helix II (Fig. 4 *B* and *C*). The 4′-phosphopantetheine arm is orientated into the VinK active site through the binding tunnel. Thus, this VinK–VinL complex structure is mechanistically reasonable for the reaction. The maleimide groups were observed to be covalently attached to both the side-chain sulfhydryl group of the mutated Cys-266 residue of VinK and the terminal sulfhydryl group of the 4′-phosphopantetheine arm of VinL, although its electron density was not clearly defined probably because of its flexibility (Fig. 4*B*). The 4′-phosphopantetheine linker region exhibits only a few interactions with VinK. The β-alanine moiety of the 4′-phosphopantetheine linker is stacked between Tyr-72 and Met-211. The hydroxy group of the 4′-phosphopantetheine linker forms a hydrogen bond with Ser-295 of VinK.

Interactions Between VinK and VinL. In the complex structure, VinL primarily contacts the small domain of VinK (Fig. 4*A*). The interface between VinK and VinL comprises ∼650 Å^2, representing 12.6% of the surface area of VinL and 5.1% of the surface area of VinK. This small contact area, which is similar to those of other enzyme–CP complex structures such as the FabA–AcpP structure (17, 18), is consistent with the transient nature of the enzyme–ACP interactions. Arg-153 and -299 of VinK form salt bridges with Glu-47 and Asp-35 of VinL, respectively (Fig. 4*C*). Met-206 of VinK extends into a hydrophobic pocket formed by Thr-39, Leu-43, Leu-59, and Phe-64 of VinL. Thus, VinK seems to recognize the helix II region of VinL through salt bridges and hydrophobic contacts.

To confirm that these salt bridges and hydrophobic contacts are functional interactions with VinL, we constructed VinK R153A, M206A, and R299A mutants and then analyzed their abilities to interact with VinL by isothermal titration calorimetry (ITC). The VinK wild type was shown to bind VinL with a K_a value of $8.2 \pm 0.8 \times 10^4$ M^{-1} (Table 1 and Fig. S4*A*), which is similar to the affinities of other MCATs for ACPs (19, 20). The R153A, M206A, and R299A mutants showed significantly reduced affinity for VinL (Fig. S4 *B*–*D*). We also carried out cross-linking assays to evaluate the interaction of each VinK mutant with VinL. The S266C/R153A, S266C/M206A, and S266C/R299A mutants all had significantly reduced cross-linking efficiency (Fig. S5*A*), consistent with the ITC results. Furthermore, we mutated VinL counterpart residues such as Asp-35 and Glu-47 and analyzed by ITC and cross-linking experiments. VinL D35A and E47A mutants showed weaker affinity (Table 1 and Fig. S4 *E* and *F*) and reduced cross-linking efficiency (Fig. S5*B*), as in the cases of VinK mutants. Thus, these mutational results showed that the presence of Arg-153, Met-206, and Arg-299 of VinK is crucial for the interaction with VinL, supporting the structural observation of the VinK–VinL complex.

Interactions Between VinK and VinP1LdACP. We next investigated the interactions between VinK and VinP1LdACP by ITC. However, the VinK wild type showed a significantly low affinity for VinP1LdACP (Fig. S4*G*), which made it difficult to calculate accurate thermodynamic parameters. Therefore, we decided to evaluate the interactions of the VinK mutants with VinP1LdACP by cross-linking assays. Among the VinK mutants, the S266C/R299A

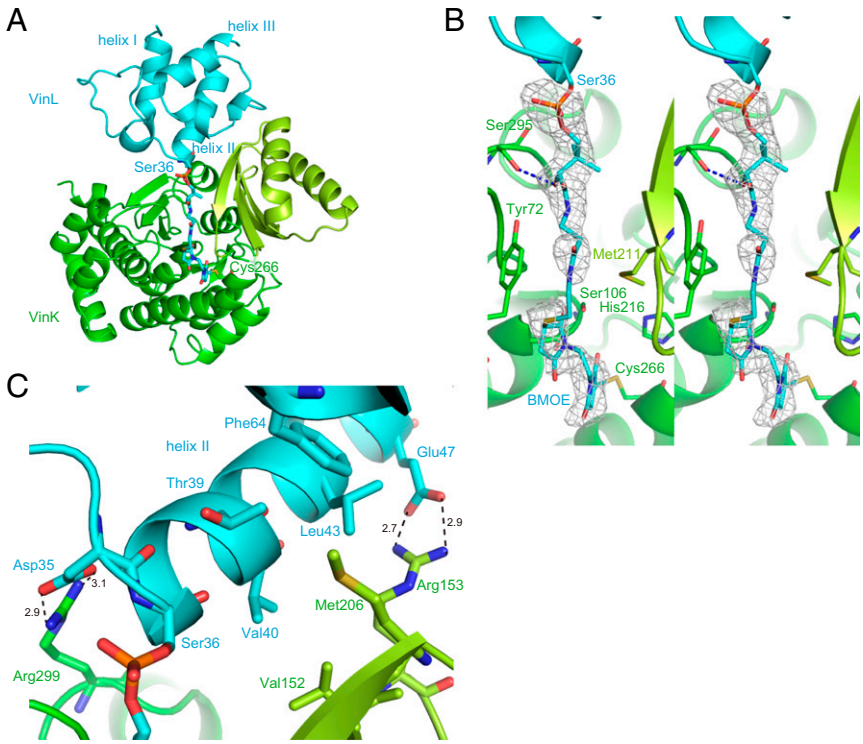

Fig. 4. Structure of the VinK–VinL complex. The VinK large domain, VinK small domain, and VinL are shown in green, yellow-green, and cyan, respectively. (*A*) Overall structure of the VinK–VinL complex. Ser-36 of VinL, 4′-phosphopantetheine arm, BMOE, and Cys-266 of VinK are shown as sticks. (*B*) Stereoview of substrate-binding tunnel region in the VinK–VinL complex. An $F_o - F_c$ electron density map contoured at 2.5σ was constructed before incorporation of the BMOE and 4′-phosphopantetheine moieties. (*C*) The binding interface between VinK and VinL. Salt-bridge interactions are shown as broken lines.

mutant had significantly decreased cross-linking efficiency compared with the S266C mutant (Fig. S5*C*), suggesting that Arg-299 of VinK is important for the interaction with VinP1LdACP. Given that Asp-35 of VinL is equivalent to Asp-86 of VinP1LdACP (Fig. S6*A*), Arg-299 might interact with Asp-86 of VinP1LdACP. In contrast, the VinK S266C/R153A and S266C/M206A mutants showed similar levels of efficiency to the S266C mutant, suggesting that Arg-153 and Met-206 do not largely interact with VinP1LdACP. This result may be explained by the fact that most of the VinL residues important for the interaction with Arg-153 and Met-206 of VinK are not conserved in VinP1LdACP. Thr-39, Leu-43, and Glu-47 of VinL are substituted with Ala-90, His-94, and Thr-98 of VinP1LdACP, respectively (Fig. S6*A*). Thus, VinP1LdACP appears to have a decreased number of salt bridges and hydrophobic interactions with VinK, likely leading to its lower affinity to VinK.

One-Pot Enzymatic Reaction of VinK Wild Type and Mutants. To compare activities of VinK wild type and mutants, we assayed their transacylation activities by a one-pot enzymatic reaction. Incubation of VinK wild type with VinN, VinO, VinM, VinL, VinP1LdACP, and associated substrates gave dipeptidyl–VinP1LdACP efficiently (Fig. S7). In contrast, all three VinK mutants showed significantly reduced formation of dipeptidyl–VinP1LdACP. Thus, disruption of interaction between VinK and VinL resulted in the decreased transacylation activity of VinK.

Discussion

The proper protein–protein interactions between CP and its partner enzyme are essential for efficient enzyme turnover in the biosynthesis of fatty acids, polyketides, and nonribosomal peptides. The binding affinities of CP for its partner enzymes are weak, enabling it to interact reversibly with each enzyme in the biosynthetic pathway (9). Because of these weak and transient interactions, structural characterization of the enzyme–CP complex is difficult. Recently, several methods using synthetic probes to capture CP in functional association with a partner enzyme were developed, allowing the structural characterization of these complexes to visualize the protein–protein interactions (17, 21–23). However, no crystal

Table 1. Affinity of VinK to VinL determined by ITC

VinK	VinL	$K_a \times 10^3$,* M^{-1}	ΔG, kcal/mol	ΔH, kcal/mol*	$-T\Delta S$, kcal/mol	*n*
Wild type	Wild type	82.1 ± 7.7	−6.7	−8.4 ± 0.2	1.7	1.11 ± 0.02*
R153A	Wild type	1.9 ± 0.0	−4.4	−6.3 ± 0.1	1.9	1.0†
M206A	Wild type	6.2 ± 0.2	−5.1	−5.5 ± 0.1	0.4	1.0†
R299A	Wild type	0.8 ± 0.1	−4.0	−5.6 ± 0.3	1.6	1.0†
Wild type	D35A	12.0 ± 0.6	−5.6	−6.7 ± 0.1	1.1	1.0†
Wild type	E47A	10.9 ± 0.5	−5.5	−7.9 ± 0.1	2.4	1.0†

*Values are ± SD from the fit.
†*n* was fixed at 1 for the purposes of fitting the data because the affinity was below the level for accurate determination of binding stoichiometry.

structure of an AT–ACP complex was reported to date. Recently, Whicher et al. described the electron cryomicroscopy structure of modular PKS PikAIII that the ACP domain is positioned near the AT domain (24). Although the phosphopantetheinylated Ser residue of ACP domain is directed toward the AT active site in this structure, the distance between them is 35 Å, which is not close enough for the acyltransfer reaction. Thus, the exact AT–ACP contact interface remains elusive.

Wong et al. described the preparation of a covalent DSZS AT–ACP complex using cross-linkers such as 1,3-dibromopropanone and BMOE (15). Their method seems to be useful to capture ACP for the crystallization of the AT–ACP complex. However, only a modest fraction of DSZS AT was cross-linked to ACP. In this study, we attempted to obtain covalent VinK–ACP complexes using BMOE as a cross-linker. Although our strategy is similar to the previous DSZS AT cross-linking experiment (15), we changed the Cys mutation position for the cross-linking reaction. The catalytic Ser-86 of DSZS AT, which corresponds to Ser-106 in VinK, was mutated to Cys in the previous cross-linking experiment, whereas we selected the noncatalytic Ser-266 located at the base of the substrate-binding tunnel. In the VinK structure, Ser-266 is placed 5 Å deeper from the entrance of the tunnel compared with the catalytic Ser-106 (Fig. 2*B*). Therefore, we expected the S266C mutant to accommodate the BMOE molecule between the mutated Cys-266 residue and the 4′-phosphopantetheine arm of VinL. We obtained the covalent VinK–ACP complexes using BMOE in sufficient yield for crystallization (Fig. 3). We also succeeded in the determination of the VinK–VinL complex structure, which, to our knowledge, is the first crystal structure of an AT–ACP complex (Fig. 4). Thus, bifunctional maleimide reagents such as BMOE are useful tools to trap the transient AT–ACP complex for structural characterization. This cross-linking reaction requires only the 4′-phosphopantetheine arm of ACP and a Cys residue at the appropriate position of the partner enzyme. Therefore, this cross-linking strategy using bifunctional maleimide reagents would be a versatile method for trapping other enzyme–ACP complexes.

Most ATs accept acyl–CoAs as substrates and transfer the acyl group to the partner ACPs. In the complex structure of *E. coli* FabD with malonyl–CoA, Arg-190, which is located at the positively charged surface near the entrance of the substrate-binding tunnel, interacts with the phosphate group of the ribose moiety of CoA (14). The acyl–CoA-specific ATs generally have an Arg or Lys residue at this position (Fig. S1). At the corresponding position, VinK has Met-206, which interacts with the hydrophobic residues of VinL (Fig. S8). VinK homolog enzymes involved in the biosynthesis of other macrolactam antibiotics also have Met or Leu residues (Fig. S1). Furthermore, acyl–ACP-specific ATs such as ZmaA and ZmaF contain a Met residue at this position (4). Thus, the presence of a hydrophobic residue at this position might be a conserved feature in acyl–ACP-specific ATs.

Helix II of several ACPs was observed to be involved in an interaction with their partner enzymes in the complex structures (9, 17, 18, 25–28). In terms of the interaction of AT with ACP, *Streptomyces coelicolor* MCAT was suggested to recognize the helix II of FAS ACP, based on the previous docking and mutational studies (19). However, the details of the binding and binding interface remain elusive. In this study, the VinK–VinL complex structure clearly shows the interaction of VinK with the negatively charged helix II region of VinL (Fig. 4*B*), which is, to our knowledge, the first direct evidence for the helix II recognition of ACP by AT. Compared with VinL, VinP1LdACP has a less acidic helix II and seems to make fewer interactions with VinK. Because VinK showed a much weaker affinity for VinP1LdACP than VinL, VinP1LdACP itself might not be enough to establish the interaction with VinK. The presence of other domains of modular VinP1PKS might affect the binding of VinK to the VinP1LdACP region in the actual vicenistatin biosynthetic pathway. Although it was suggested from the VinK–VinL structure that the negatively charged helix II region of ACP is used for the recognition by AT, it is still unclear whether this binding model can be applied to all cases of AT–ACP interaction. Some PKS ATs are predicted to bind ACP in a different manner based on docking analysis. For example, *S. coelicolor* MCAT was suggested to interact with the loop region between helix I and II of actinorhodin PKS ACP (19, 29). Alternatively, the presence of an additional domain such as the KS-AT linker domain in modular PKS might be involved in the binding mode of ACP, as proposed in the interaction between AT_{DYN10} and ACP_{DYN} involved in dynemicin biosynthesis (30). For complete understanding of ACP recognition by AT, it is necessary to obtain other AT–ACP complex structures.

In conclusion, we succeeded in obtaining, to our knowledge, the first crystal structure of an AT–ACP complex. This complex structure should be useful for the prediction of a model for other AT–ACP complex interactions. This study could provide useful clues for the engineering of ATs to optimize protein–protein interactions with ACP for production of unnatural polyketide products.

Materials and Methods

VinK, VinL, and VinP1LdACP proteins were expressed and purified as described (12). VinK mutants were prepared by site-directed mutagenesis. The cross-linking reactions were performed in the presence of BMOE (Thermo Fisher Scientific). VinK protein and the VinK–VinL complex were crystallized by using the vapor-diffusion method. The VinK structure was solved by the single-wavelength anomalous dispersion method. ITC experiments were carried out at 25 °C by using the MicroCal iTC200 (GE Healthcare). The details for all of the experimental protocols are described in *SI Materials and Methods*.

ACKNOWLEDGMENTS. This work was performed with the approval of the Photon Factory Program Advisory Committee (Proposals 2012G508 and 2014G530) and was supported in part by Japan Society for the Promotion of Science Grants-in-Aid for Young Scientists (B) 15K18679 (to A.M.); and Ministry of Education, Culture, Sports, Science and Technology Grants-in-Aid for Scientific Research in Innovative Areas 22108003 (to T.E.).

1. Hertweck C (2009) The biosynthetic logic of polyketide diversity. *Angew Chem Int Ed Engl* 48(26):4688–4716.
2. Piel J (2010) Biosynthesis of polyketides by trans-AT polyketide synthases. *Nat Prod Rep* 27(7):996–1047.
3. Chan YA, Podevels AM, Kevany BM, Thomas MG (2009) Biosynthesis of polyketide synthase extender units. *Nat Prod Rep* 26(1):90–114.
4. Park H, Kevany BM, Dyer DH, Thomas MG, Forest KT (2014) A polyketide synthase acyltransferase domain structure suggests a recognition mechanism for its hydroxymalonyl-acyl carrier protein substrate. *PLoS One* 9(10):e110965.
5. Dunn BJ, Khosla C (2013) Engineering the acyltransferase substrate specificity of assembly line polyketide synthases. *J R Soc Interface* 10(85):20130297.
6. Liou GF, Khosla C (2003) Building-block selectivity of polyketide synthases. *Curr Opin Chem Biol* 7(2):279–284.
7. Wong FT, Chen AY, Cane DE, Khosla C (2010) Protein-protein recognition between acyltransferases and acyl carrier proteins in multimodular polyketide synthases. *Biochemistry* 49(1):95–102.
8. Ye Z, Musiol EM, Weber T, Williams GJ (2014) Reprogramming acyl carrier protein interactions of an Acyl-CoA promiscuous trans-acyltransferase. *Chem Biol* 21(5):636–646.
9. Crosby J, Crump MP (2012) The structural role of the carrier protein–active controller or passive carrier. *Nat Prod Rep* 29(10):1111–1137.
10. Kudo F, Miyanaga A, Eguchi T (2014) Biosynthesis of natural products containing β-amino acids. *Nat Prod Rep* 31(8):1056–1073.
11. Shindo K, Kamishohara M, Odagawa A, Matsuoka M, Kawai H (1993) Vicenistatin, a novel 20-membered macrocyclic lactam antitumor antibiotic. *J Antibiot (Tokyo)* 46(7):1076–1081.
12. Shinohara Y, Kudo F, Eguchi T (2011) A natural protecting group strategy to carry an amino acid starter unit in the biosynthesis of macrolactam polyketide antibiotics. *J Am Chem Soc* 133(45):18134–18137.
13. Miyanaga A, Cieślak J, Shinohara Y, Kudo F, Eguchi T (2014) The crystal structure of the adenylation enzyme VinN reveals a unique β-amino acid recognition mechanism. *J Biol Chem* 289(45):31448–31457.
14. Oefner C, Schulz H, D'Arcy A, Dale GE (2006) Mapping the active site of *Escherichia coli* malonyl-CoA-acyl carrier protein transacylase (FabD) by protein crystallography. *Acta Crystallogr D Biol Crystallogr* 62(Pt 6):613–618.
15. Wong FT, Jin X, Mathews II, Cane DE, Khosla C (2011) Structure and mechanism of the trans-acting acyltransferase from the disorazole synthase. *Biochemistry* 50(30):6539–6548.

16. Roujeinikova A, et al. (2007) Structural studies of fatty acyl-(acyl carrier protein) thioesters reveal a hydrophobic binding cavity that can expand to fit longer substrates. *J Mol Biol* 365(1):135–145.
17. Nguyen C, et al. (2014) Trapping the dynamic acyl carrier protein in fatty acid biosynthesis. *Nature* 505(7483):427–431.
18. Lohman JR, et al. (2014) The crystal structure of BlmI as a model for nonribosomal peptide synthetase peptidyl carrier proteins. *Proteins* 82(7):1210–1218.
19. Arthur CJ, et al. (2009) Structure and malonyl CoA-ACP transacylase binding of *streptomyces coelicolor* fatty acid synthase acyl carrier protein. *ACS Chem Biol* 4(8): 625–636.
20. Zhang L, et al. (2007) Malonyl-CoA: Acyl carrier protein transacylase from *Helicobacter pylori*: Crystal structure and its interaction with acyl carrier protein. *Protein Sci* 16(6):1184–1192.
21. Sundlov JA, Shi C, Wilson DJ, Aldrich CC, Gulick AM (2012) Structural and functional investigation of the intermolecular interaction between NRPS adenylation and carrier protein domains. *Chem Biol* 19(2):188–198.
22. Haslinger K, et al. (2014) The structure of a transient complex of a nonribosomal peptide synthetase and a cytochrome P450 monooxygenase. *Angew Chem Int Ed Engl* 53(32):8518–8522.
23. Finzel K, Lee DJ, Burkart MD (2015) Using modern tools to probe the structure-function relationship of fatty acid synthases. *ChemBioChem* 16(4):528–547.
24. Whicher JR, et al. (2014) Structural rearrangements of a polyketide synthase module during its catalytic cycle. *Nature* 510(7506):560–564.
25. Cryle MJ, Schlichting I (2008) Structural insights from a P450 carrier protein complex reveal how specificity is achieved in the P450(BioI) ACP complex. *Proc Natl Acad Sci USA* 105(41):15696–15701.
26. Parris KD, et al. (2000) Crystal structures of substrate binding to *Bacillus subtilis* holo-(acyl carrier protein) synthase reveal a novel trimeric arrangement of molecules resulting in three active sites. *Structure* 8(8):883–895.
27. Babu M, et al. (2010) Structure of a SLC26 anion transporter STAS domain in complex with acyl carrier protein: Implications for *E. coli* YchM in fatty acid metabolism. *Structure* 18(11):1450–1462.
28. Guy JE, et al. (2011) Remote control of regioselectivity in acyl-acyl carrier protein-desaturases. *Proc Natl Acad Sci USA* 108(40):16594–16599.
29. Keatinge-Clay AT, et al. (2003) Catalysis, specificity, and ACP docking site of *Streptomyces coelicolor* malonyl-CoA:ACP transacylase. *Structure* 11(2):147–154.
30. Liew CW, et al. (2012) Crystal structure of the acyltransferase domain of the iterative polyketide synthase in enediyne biosynthesis. *J Biol Chem* 287(27):23203–23215.
31. Battye TG, Kontogiannis L, Johnson O, Powell HR, Leslie AG (2011) iMOSFLM: A new graphical interface for diffraction-image processing with MOSFLM. *Acta Crystallogr D Biol Crystallogr* 67(Pt 4):271–281.
32. Terwilliger TC, et al. (2009) Decision-making in structure solution using Bayesian estimates of map quality: The PHENIX AutoSol wizard. *Acta Crystallogr D Biol Crystallogr* 65(Pt 6):582–601.
33. Langer G, Cohen SX, Lamzin VS, Perrakis A (2008) Automated macromolecular model building for X-ray crystallography using ARP/wARP version 7. *Nat Protoc* 3(7): 1171–1179.
34. Vagin A, Teplyakov A (2010) Molecular replacement with MOLREP. *Acta Crystallogr D Biol Crystallogr* 66(Pt 1):22–25.
35. Emsley P, Cowtan K (2004) Coot: Model-building tools for molecular graphics. *Acta Crystallogr D Biol Crystallogr* 60(Pt 12 Pt 1):2126–2132.
36. Murshudov GN, Vagin AA, Dodson EJ (1997) Refinement of macromolecular structures by the maximum-likelihood method. *Acta Crystallogr D Biol Crystallogr* 53(Pt 3): 240–255.
37. Krissinel E, Henrick K (2007) Inference of macromolecular assemblies from crystalline state. *J Mol Biol* 372(3):774–797.
38. Lovell SC, et al. (2003) Structure validation by Calpha geometry: ϕ,ψ and Cbeta deviation. *Proteins* 50(3):437–450.
39. Morris GM, et al. (2009) AutoDock4 and AutoDockTools4: Automated docking with selective receptor flexibility. *J Comput Chem* 30(16):2785–2791.
40. Schüttelkopf AW, van Aalten DMF (2004) PRODRG: A tool for high-throughput crystallography of protein-ligand complexes. *Acta Crystallogr D Biol Crystallogr* 60(Pt 8):1355–1363.